

# Hydrogen diffusion in hydrogenated Mg and Mg-Mg<sub>2</sub>Ni eutectic alloy

J. Čermák\*, L. Král, I. Stloukal

*Institute of Physics of Materials AS CR, v. v. i., Žižkova 22, CZ-616 62 Brno, Czech Republic*

Received 3 October 2007, received in revised form 6 November 2007, accepted 7 November 2007

## Abstract

Time dependence of total amount of hydrogen desorbed from hydrogen-charged Mg and eutectic Mg-Mg<sub>2</sub>Ni (23.5 wt.% Ni) alloy was measured at temperatures from interval 552–723 K. Experiments were carried out well below the equilibrium pressure, where these hydrides – perspective as solid hydrogen storage media – are unstable and the desorption process is controlled mainly by diffusion of hydrogen in respective hydride (MgH<sub>2</sub> and/or Mg<sub>2</sub>NiH<sub>4</sub>). Hydrogen diffusion coefficients were evaluated from desorption curves and hydrogen diffusion coefficient along interphase boundary MgH<sub>2</sub>/Mg<sub>2</sub>NiH<sub>4</sub> was estimated from results obtained with the eutectic alloy.

**Key words:** intermetallic phases, magnesium, magnesium alloys, diffusion, hydrogen diffusion, hydrogen storage

## 1. Introduction

Magnesium and its alloys had been frequently studied as construction materials [1] for applications, where the mechanical strength, creep and fatigue resistivity are of prime importance [2–10]. In the last decade, however, they became also important due to their large potential as hydrogen-storage materials (HSMs) since hydrogen is a very prospective fuel both for direct combustion and in electrochemical batteries and fuel cells. Contrary to the fact that there is a broad variety of materials suitable as HSMs (for review see, e.g. in [11–13]), magnesium-based alloys play a prominent role because of two main reasons: First, magnesium is a very cheap and abundant element on the Earth, and second, the light Mg-based matrix enables to achieve the best (up to now) weight storage ratio. Before all, eutectic mixtures Mg + Mg<sub>2</sub>Ni and pure Mg<sub>2</sub>Ni intermetallic compound are in the focus of interest as base materials. Even alloyed, Mg-based HSMs need temperatures about 470 K for charging/decharging (C/D) cycle, which makes them a little bit uncomfortable for energy sources in personal and household appliances. Considerable effort is, therefore, constantly devoted to lowering the sta-

bility of Mg-based hydrides, to preserve their favorable storage capacity and at the same time, to enhance the rate of C/D kinetics – see e.g., in [14–19].

Though there are some studies of hydrogen C/D kinetics in Mg-based alloys [20–28], the rate constants are known only. Contrary to often drawn conclusion, namely that the process of hydrogen desorption is controlled by diffusion [20, 21, 24, 29], quantitative data describing hydrogen diffusion itself are very sparse in the literature. For example in paper [23], the authors declare the  $\alpha/\beta$  ( $\alpha$  – base matrix with hydrogen solved,  $\beta$  – hydride) interphase motion at high temperatures, nucleation-and-growth at “early stages” and diffusion at “later stages” as respective controlling mechanisms. In ref. [24, 26], authors tested a number of known rate equations and chose “the best one” for their materials studied. It should be noted, however, that the choice of the optimal equation (and the probable kinetic mechanism governing the respective phase change) is, in this way, very difficult. It is also known that Mg<sub>2</sub>NiH<sub>4</sub> compound undergoes a phase change between the room temperature and the melting point [30–40], which complicates the kinetic study of C/D processes in the material.

The aim of the present study is to obtain diffusion

\*Corresponding author: tel.: +420 532290422; fax: +420 541218657; e-mail address: [cermak@ipm.cz](mailto:cermak@ipm.cz)

coefficients of hydrogen in hydrogen charged Mg (i. e. in  $\text{MgH}_2$ ), and in hydrogen charged eutectic ( $\text{Mg} + \text{Mg}_2\text{Ni}$ )-H. The results may enable to quantify the rate of hydrogen-diffusion-controlled processes running in these materials, which are often used as a base of HSMs.

## 2. Experimental

### 2.1. Experimental materials

Experimental alloys were prepared from pure components 3N6Ni and 3N8Mg. Splinters of pure components for eutectic alloy were ball-milled in air using *Fritsch-Pulverisette6*. The composition was Mg-23.5wt.%Ni. Thickness of splinters was about 0.1 mm and the milling conditions were following: mass ratio of balls to that of the milled mixture  $r_m = 25$  and milling time regime: 10 min milling + 50 min relaxation – 20 times repeated. Milled powder was pressure-compacted at room temperature into pellets with diameter 20 mm  $\times$  5 mm in height.

Samples from pure Mg and from cast modification of eutectic alloy were prepared by induction melting in the MgO crucible under Ar protective atmosphere. Ingots were cut into slices about 2 mm thick that were ground with metallographic papers down to foils of final thickness 2l lying between 100 and 704  $\mu\text{m}$ .

For the sake of comparison, desorption experiments were done also with compacted powder of  $\text{MgH}_2$  (98 %) purchased in Alfa Aesar Germany. The mean grain size of particles  $2\rho$  was about 100  $\mu\text{m}$ .

### 2.2. Hydrogen charging

Hydrogen charging followed immediately after the pellets/foils preparation by isothermal annealing in a pressure vessel. Pressure of pure (5N3) hydrogen was 30 bars and the charging temperature was  $T_c = 673$  K. The time of charging was several hours by pellets and 14 days by foils. In the case of eutectic alloy, a complete charging was achieved – no further increase in hydrogen content in samples was observed after additional charging, which was monitored by precise weighing. The foils of pure magnesium were covered by a compact layer of hydride.

### 2.3. SEM observation

#### 2.3.1. Pellets

The structure of samples was checked by SEM JEOL JSM 6460 equipped with EDAX/WEDAX Oxford Instruments analyzer. Samples were porous and consisted of compact grains of mean size  $2\rho$  most frequently between 10 and 50  $\mu\text{m}$  as it is illustrated in

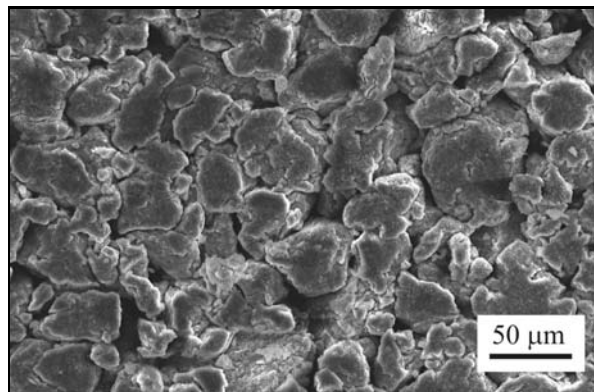


Fig. 1. Structure of compacted pellets of eutectic alloy after the hydrogen charging.

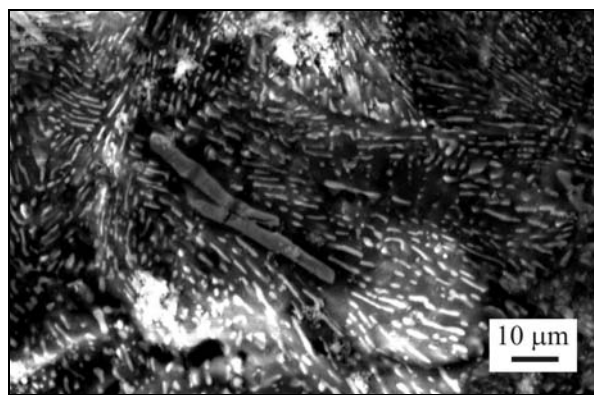


Fig. 2. SEM micrograph of cast eutectic alloy after the hydrogen charging. Light particles and lamellae –  $\text{Mg}_2\text{NiH}_4$ .

Fig. 1. Mean grain size of hydrogen charged pellets was reduced somewhat due to fragmentation of the largest grains. Chemical composition of grains coincided well with the intended average composition of eutectic alloy.

#### 2.3.2. Foils

The microstructure of cast eutectic alloy is shown in Fig. 2. It consists of oblong  $\text{Mg}_2\text{Ni}$  particles (size about  $40 \times 3 \mu\text{m}$ ) in lamellar eutectic matrix (inter-lamellar distance is about 2  $\mu\text{m}$ ). After the hydrogen charging, the  $\text{MgH}_2$  matrix accommodates the strains between the  $\text{Mg}_2\text{NiH}_4$  lamellae and, therefore, hydrogen charging of eutectic alloy does not lead to cracking.

Grain size of Mg ingot was in the order of tens of mm. Hence, it can be presumed that the presence of grain boundaries in Mg does not influence significantly the kinetics of the C/D process.  $\text{MgH}_2$  hydride phase started to grow from separated nuclei at the surface of the foils (see Fig. 3) and the further growth of the phase proceeded mainly in lateral directions. After

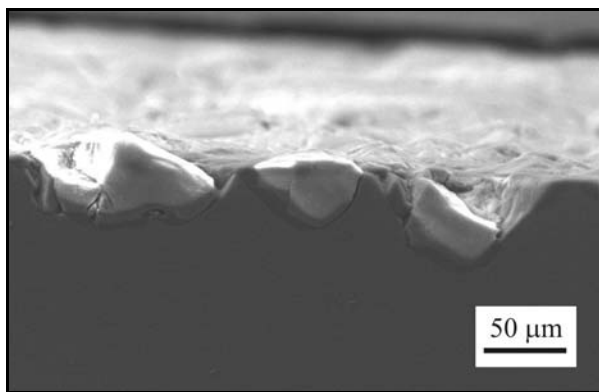


Fig. 3. SEM micrograph of transversal cut of cast Mg foil after early stages of hydrogen charging. Growing  $\text{MgH}_2$  nuclei at the surface.

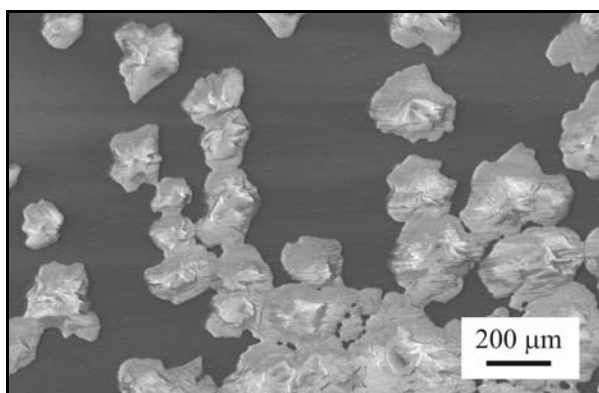


Fig. 4. SEM micrograph of the surface of cast Mg foil after early stages of hydrogen charging. Progressive coalescence of growing  $\text{MgH}_2$  islands at the surface.

the coalescence of hydride islands (Fig. 4), the compact hydride layer of irregular thickness was formed on both surfaces of the foils (Fig. 5) and its further growth was very slow. Mean thickness of the layer  $l$  was estimated via SEM image analysis of the transversal cuts of foils.

#### 2.4. XRD phase analysis

X-ray profiles were obtained by X'Pert Pro MPD device (PANalytical B. V., Almelo, the Netherlands) using  $\text{Co K}\alpha$  radiation and interpreted by the HighScore Plus software with commercial databases [41–43].

The results can be illustrated by the most significant reflections marked in XRD pattern shown in Fig. 6. Hydrogen charged Mg foils (Fig. 6a) contain exclusively Mg and  $\text{MgH}_2$  phases, whereas decharged Mg samples (Fig. 6b) show Mg lines only. Prevailing phase in charged eutectic alloy are  $\text{Mg}_2\text{NiH}_4$ ,  $\text{MgH}_2$  and  $\text{Mg}_2\text{NiH}_{0.3}$  (Fig. 6c). No traces of magnesium ox-

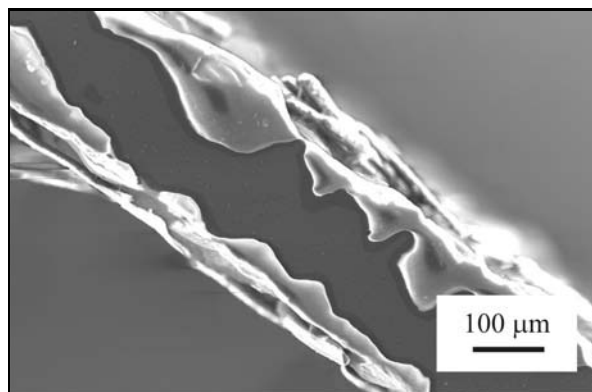


Fig. 5. Transversal cut of cast Mg foil – final stages of hydrogen charging. Continuous  $\text{MgH}_2$  layer of irregular thickness  $l$  at both surfaces slows down further hydrogenation.

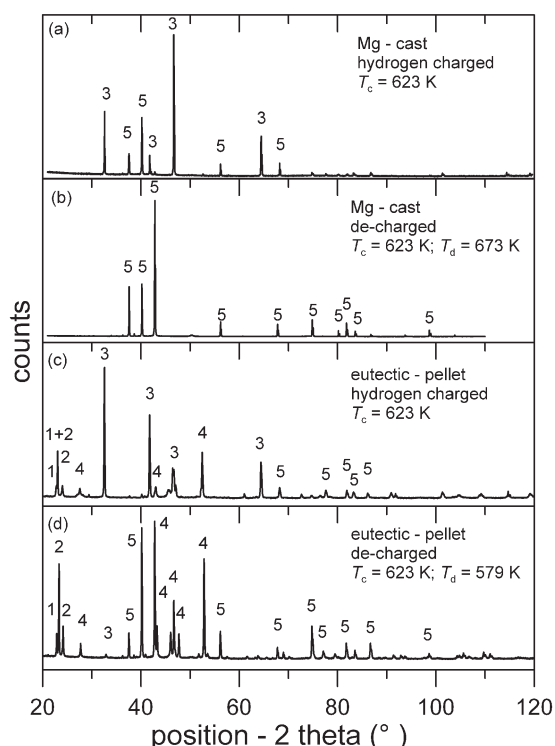


Fig. 6. XRD pattern of Mg and eutectic alloy: 1 –  $\text{Mg}_2\text{NiH}_4$ , 2 –  $\text{Mg}_2\text{NiH}_{0.3}$ , 3 –  $\text{MgH}_2$ , 4 –  $\text{Mg}_2\text{Ni}$ , 5 – Mg;  $T_c$  – charging temperature,  $T_d$  – decharging temperature.

ide and magnesium hydroxides were detected in experimental samples.

#### 2.5. Mass spectroscopy

A semi-quantitative analysis of gaseous phase desorbed from the studied samples was carried out at Masaryk University Brno, Czech Republic using quad-

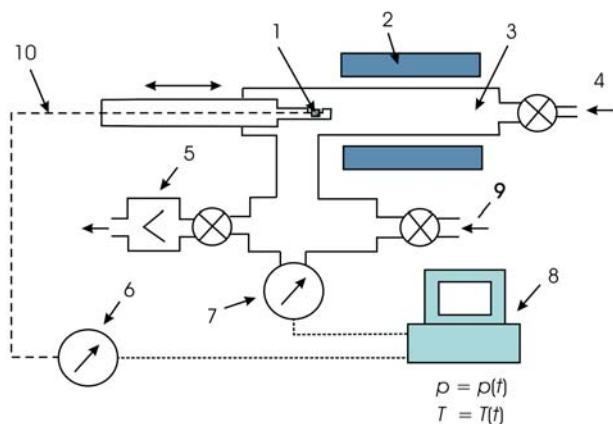


Fig. 7. Experimental apparatus – schematically: 1 – sample, 2 – furnace, 3 – vacuum chamber, 4 – hydrogen inlet, 5 – vacuum pump, 6 – mV-meter, 7 – vacuum gauge, 8 – PC, 9 – venting, 10 – thermocouple Pt-PtRh.

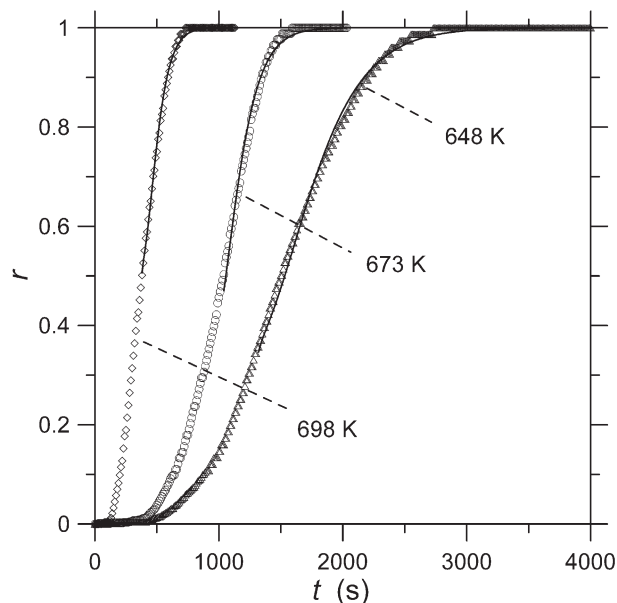


Fig. 8. Desorption curves measured in cast Mg foils with  $l = 49 \mu\text{m}$ , charged at  $T_c = 623 \text{ K}$ . Decharging temperature  $T_d = 648\text{--}698 \text{ K}$ . Full lines – Eq. (2).

rupole mass spectrometer TRIO 1000 Fisons Instrument, Finnigan MAT.

Negligibly small traces of residual air were detected in mass channels 28 ( $\text{N}_2$ ), 32 ( $\text{O}_2$ ) and weak traces in channels 18 ( $\text{H}_2\text{O}$ ), 40 ( $\text{Ar}$ ) and 44 ( $\text{CO}_2$ ) by scanning analysis (dependence of signal intensity on the temperature in temperature interval from room temperature to 673 K). Hence, the gaseous phase released between the room temperature and 673 should be identified exclusively with hydrogen (which could not be directly detected by this method).

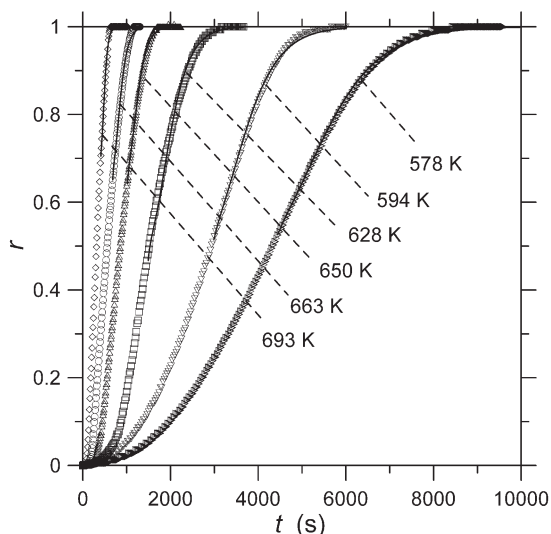


Fig. 9. Desorption curves measured with  $\text{MgH}_2$  powder with mean grain size  $2a \sim 100 \mu\text{m}$  purchased in Alfa Aesar Germany. Decharging temperature  $T_d = 578\text{--}693 \text{ K}$ . Full lines – Eq. (1).

## 2.6. Hydrogen desorption

The desorption experiments were carried out in a vacuum chamber of calibrated volume enabling heating the sample isothermally at chosen temperatures  $T_d$  and measuring the time dependence of desorbed hydrogen pressure  $p(t)$ . The thermocouple Pt/PtRh was in contact with the sample, the mass of which was typically 3 g. The arrangement is shown schematically in Fig. 7.

## 3. Results and discussion

### 3.1. Desorption curves

The measurement of desorption curves  $p = p(t)$  was done in isothermal regime. All measured desorption curves are plotted in Figs. 8–12 in co-ordinates relative pressure  $r = (p - p_s)/(p_f - p_s)$  vs time  $t$ . The starting pressure  $p_s$  was always 2 mbar and the maximum pressure  $p_f$ , reached during the desorption, ranged from 80 to 200 mbar.

### 3.2. Evaluation of diffusion coefficients

The present experiments were done in pressure interval lying well below the equilibrium pressure  $p_{\text{eq}}$  of both  $\text{MgH}_2$  and  $\text{Mg}_2\text{NiH}_4$  calculated for each desorption temperature from van't Hoff equation [44]. This assures that mobile hydrogen atoms are released in the whole volume of the hydrides (homogeneous nuc-

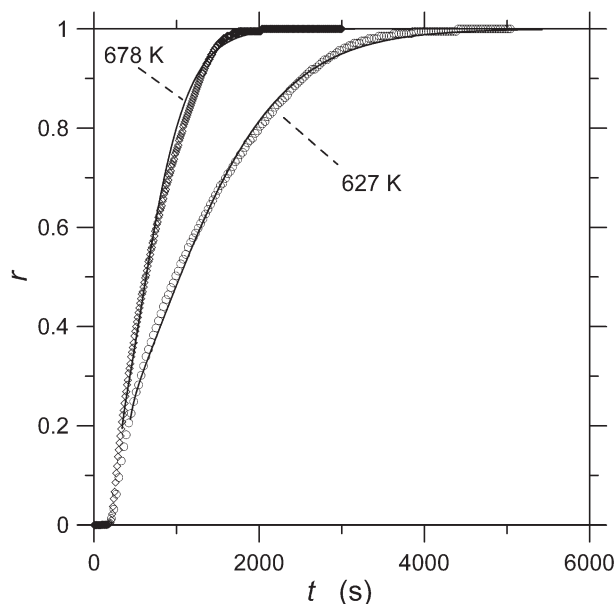


Fig. 10. Desorption curves measured with cast eutectic alloy. Foils with  $l = 198 \mu\text{m}$  charged at  $T_c = 623 \text{ K}$ . Decharging temperatures  $T_d = 627$  and  $678 \text{ K}$ . Full lines – Eq. (2).

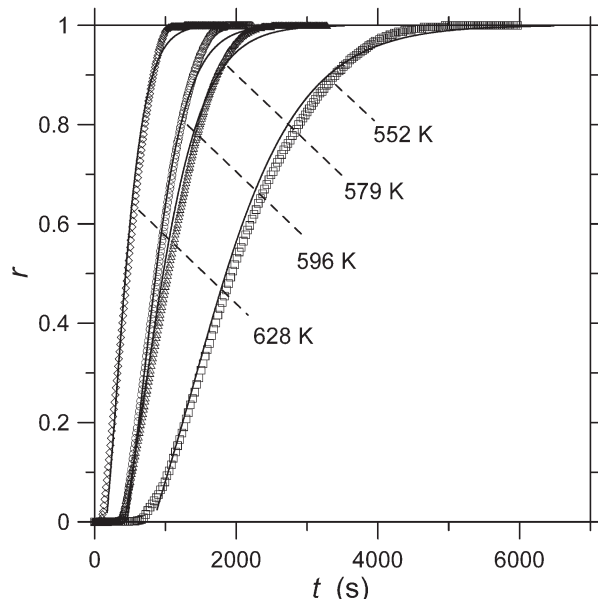


Fig. 12. Desorption curves measured with eutectic alloy – pellets. Mean grain size  $2\rho = 44 \mu\text{m}$  charged at  $T_c = 623 \text{ K}$ . Decharging temperatures  $T_d = 552$ – $628 \text{ K}$ . Full lines – Eq. (1).

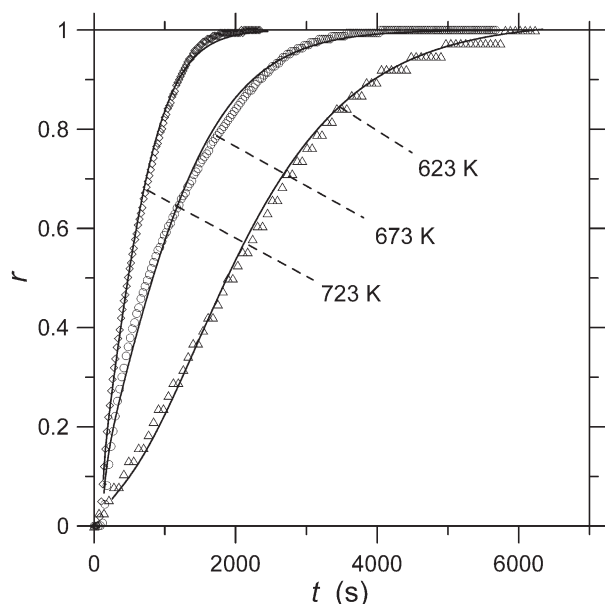


Fig. 11. Desorption curves measured with cast eutectic alloy. Foils with  $l = 352 \mu\text{m}$  charged at  $T_c = 623 \text{ K}$ . Decharging temperatures  $T_d = 623$ – $723 \text{ K}$ . Full lines – Eq. (2).

leation of  $\alpha$  phase:  $\beta \rightarrow \alpha + \text{H}$ ). Under such conditions, the hydrogen evolution from the samples can be described by equations derived for diffusion from the bulk of spatially limited bodies into the finite volume.

It is obvious from Fig. 1 that the pellets are porous agglomerates of small particles that can be quite reasonably approximated by spheres. Hence, for the rel-

ative amount of hydrogen desorbed from the samples into the limited volume,  $r = (p - p_s)/(p_f - p_s)$ , equations derived in [45, 46] for desorption from the sphere of radius  $\rho$  into “well stirred” finite volume can be used:

$$r = 1 - A \sum_{n=1}^{\infty} \frac{1}{n^2} \int_0^{t'} G(\tau) \exp \left[ -\frac{D\pi^2}{\rho^2} n^2 (t' - \tau) \right] d\tau, \quad (1)$$

where  $A$  is a constant,  $D$  is the hydrogen diffusion coefficient and the function  $G$  describes the rate of hydrogen evolution. The time  $t' = t - t_s$  in Eq. (1) is related to a start time of the desorption,  $t_s$ , which can be found as a fitting parameter.

In case of hydrogen diffusion from foils, analogous equation can be used derived for the out-diffusion from a plane sheet [45, 46]:

$$r = 1 - A \sum_{n=0}^{\infty} \frac{1}{(2n+1)^2} \cdot \int_0^{t'} G(\tau) \exp \left[ -\frac{D\pi^2}{l^2} (n+1/2)^2 (t' - \tau) \right] d\tau. \quad (2)$$

Convolution in Eqs. (1) and (2) accounts for the fact that not all hydrogen atoms are free for diffusion at  $t' = 0$ . We propose following representation of  $G$ :

Table 1. Hydrogen diffusion coefficients and values of  $\lambda$  in hydrogen charged Mg and Mg + Mg<sub>2</sub>Ni eutectic alloy obtained by fitting of Eqs. (1) and (2).  $2l$  – thickness of the foil,  $2\rho$  – mean size of particles in pellets or in MgH<sub>2</sub> powder. Hydrogen charging temperature  $T_c = 623$  K

Material	$T_d$	$D$	$\lambda$
	K	$10^{-11} \text{ m}^2 \text{ s}^{-1}$	$\text{s}^{-1}$
eutectic foils; $l = 352 \text{ } \mu\text{m}$	723	17.4	2.3
	673	8.76	1.8
	623	4.76	0.7
eutectic foils; $l = 198 \text{ } \mu\text{m}$	678	6.79	5.1
	627	2.79	2.1
eutectic pellets; $\rho = 22 \text{ } \mu\text{m}$	628	0.0295	6.4
	596	0.0197	4.0
	579	0.0148	3.0
	552	0.00786	1.3
Mg foil; $l = 49 \text{ } \mu\text{m}$	698	1.58	15
	673	0.901	10
	648	0.414	3.8
MgH <sub>2</sub> powder; $\rho = 50 \text{ } \mu\text{m}$	693	0.583	27
	663	0.278	12
	650	0.215	9
	628	0.101	11
	594	0.0607	2.4
	578	0.0380	1.5

$$G(\tau) < \frac{\delta(0)}{\lambda} \exp(-\lambda\tau). \quad (3)$$

$$\frac{1}{\lambda} \exp(-\lambda\tau). \quad (4)$$

Equation (3), where  $\delta(0)$  is the Dirac's delta function in  $\tau = 0$ , leads to the case known as *instantaneous diffusion source* [47]. It means that all hydrogen atoms in the volume of the particle are free for diffusion at  $\tau = 0$ . Equation (4) with small  $\lambda$  approaches the so-called *constant source* [47], i. e., continual generation of mobile hydrogen atoms, and medium values of  $\lambda$  allow for initial generation of mobile hydrogen atoms, which fades out with time  $\tau$ .

Fitting of the experimental data was done with several first terms only in series in Eqs. (1) and (2). Therefore, for the shortest time  $t'$ , the analytic solution does not describe properly the data. Moreover, it is obvious that Eqs. (1) and (2) were derived for single constant values of  $\rho$  and  $l$ , respectively. However, the presence of very small particles in pellets (Fig. 1) and non-regular thickness of MgH<sub>2</sub> layer on Mg foils (Fig. 5) cause that the measured desorption curves are sigmoid at the very beginning, which cannot be described by Eqs. (1) and (2). These two factors are why the data were not fitted from the time  $t' = 0$ . Nevertheless, it can be seen in Figs. 8–12 that the ex-

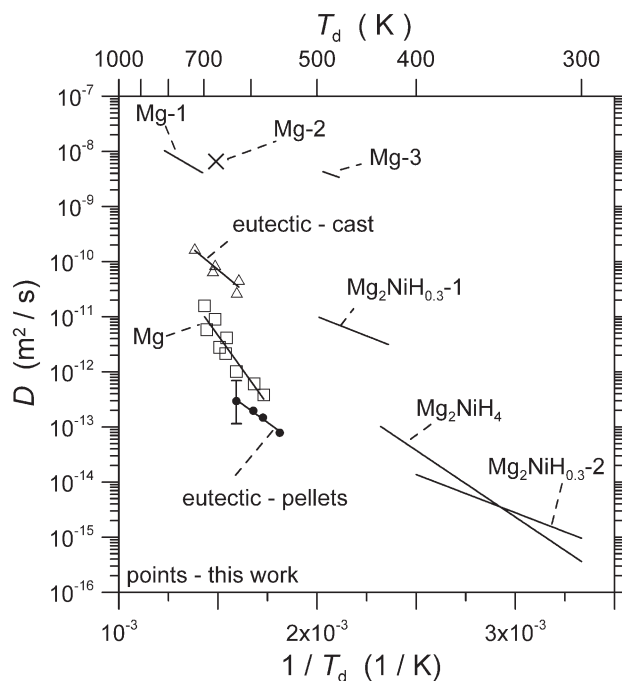


Fig. 13. Arrhenius diagram of hydrogen diffusion coefficients. Mg<sub>2</sub>NiH<sub>4</sub> [51], Mg<sub>2</sub>NiH<sub>0.3-1</sub> [52], Mg<sub>2</sub>NiH<sub>0.3-2</sub> [53], Mg-1 [48], Mg-2 [49], Mg-3 [50]. Error bar – typical experimental error.

perimental points are fitted reasonably by Eqs. (1) and (2) at sufficiently large times. Diffusion coefficients  $D$  and parameters  $\lambda$  obtained as fitting parameters are listed in Table 1.

### 3.3. Temperature dependence of $D$ and $\lambda$

Temperature dependence of diffusion coefficients,  $D$ , is shown in Fig. 13. The error bar denotes a typical accuracy of experimental points and, at the same time, it shows also an estimated uncertainty of the results following from the fact that used values of  $\rho$  and  $l$  are not constant in the samples. Hydrogen diffusion coefficients measured in charged Mg foils and those measured in MgH<sub>2</sub> powder (purchased in Alfa Aesar; average diameter of grains  $2\rho \sim 100 \text{ } \mu\text{m}$ ) agree reasonably one with another. Further, the values of hydrogen diffusion coefficients in charged Mg are much smaller compared to values reported for hydrogen diffusion in pure Mg [48–50] – cf. the present data with literature values marked as Mg-1, 2, 3 in Fig. 13. This supports the idea that the present data characterize the hydrogen diffusion in hydride  $\beta$ -phase, not in the  $\alpha$ -solid solution.

Hydrogen diffusion coefficients measured in the hydrogen charged eutectic alloy prepared by ball-milling and compacting (in pellets) differ significantly from much higher values of effective hydro-

Table 2. Arrhenius parameters of hydrogen diffusion in hydrogen-charged experimental alloys

Matrix	Q	$-\ln D_0$
	kJ mol <sup>-1</sup>	$D_0$ (m <sup>2</sup> s <sup>-1</sup> )
MgH <sub>2</sub> <sup>1)</sup>	96 ± 12	8.8 ± 2.3
hydrogen-charged eutectic	57 ± 13	13.0 ± 2.4
interphase boundary		3.4 ± 2.4 <sup>2)</sup>

<sup>1)</sup> Pellets of hydrogen-charged Mg and purchased powder MgH<sub>2</sub>. <sup>2)</sup> Calculated from Eq. (6).

gen diffusion coefficients measured in foils of cast eutectic alloy. This is, most likely, caused by the fact that the particles in pellets (Fig. 1) are formed by a compact matter, which chemical composition agrees with the average chemical composition of the eutectic. Therefore, the measured values of  $D$  characterize, in this case, the hydrogen diffusion coefficients lying between the values that could be measured in individual phases, MgH<sub>2</sub> and Mg<sub>2</sub>NiH<sub>4</sub>.

On the other hand, the cast eutectic is a heterogeneous mixture of the both phases separated by interphase boundaries (Fig. 2). Therefore, the measured value of  $D$  is influenced by the fast diffusion along the interphase boundaries. It is interesting to note that similar influence of interphase boundaries upon the measured effective value of  $D$  can be expected also by results reported in the literature, since the extrapolation of present results to low temperatures is close to literature data obtained in experiments with samples formed by a mixture of hydrides [51–53] (Fig. 13).

The calculated values of  $D$  were fitted to Arrhenius equation  $D = D_0 \exp(-Q/RT)$  ( $R$  is the gas constant) and frequency factor  $D_0$  and activation enthalpy  $Q$  was evaluated for all experimental alloys. Results are summarized in Table 2.

It is obvious from Table 1 that obtained values of  $\lambda$  increase with increasing desorption temperature  $T_d$ , which supports an expected fact that the desorption rate of hydrogen bound in hydride phase increases with increasing temperature.

### 3.4. Assessment of hydrogen diffusion coefficient in interphase boundaries

If the  $D$ 's measured in ball-milled eutectic alloy (in pellets) may be taken for an estimation of *mean* hydrogen diffusion coefficient in both phases MgH<sub>2</sub>, Mg<sub>2</sub>NiH<sub>4</sub> and  $D$ 's measured in cast eutectic for an effective value  $D_{\text{eff}}$  in two-phase alloy with interphase boundaries, it is possible to assess the hydrogen diffusion coefficient in the interphase boundary,  $D_i$ , using the theory published in paper [54]. For the effective

diffusion coefficient  $D_{\text{eff}}$ , the authors derived relation:

$$D_{\text{eff}} = \frac{D_i}{g_i + \frac{g_1}{s_1} + \frac{g_2}{s_2}} \cdot \frac{1 - 2g_1 \frac{D_i s_1 - D_1}{2D_i s_1 + D_1} - 2g_2 \frac{D_i s_2 - D_2}{2D_i s_2 + D_2}}{1 + g_1 \frac{D_i s_1 - D_1}{2D_i s_1 + D_1} + g_2 \frac{D_i s_2 - D_2}{2D_i s_2 + D_2}}, \quad (5)$$

which can be simplified if (i) the diffusion coefficient in interphase boundary,  $D_i$ , is much greater than in both phases ( $D_i \gg D_1, D_2$ ) and (ii) the segregation of hydrogen to interphase boundaries is negligible ( $s_1 \delta \sim s_2 \delta \sim s \delta \ll 1$  and  $s \sim 1$ ;  $s_{1,2}$  – hydrogen segregation factors to interfaces phase 1/matrix and phase 2/matrix respectively,  $\delta$  – thickness of the interphase boundary). Symbols  $g_i, g_1, g_2$  ( $g_i \ll g_1, g_2$ ) in Eq. (5) stand for volume fractions of interphase boundary and both phases, respectively. The simplification leads to an approximate relation enabling an estimation of hydrogen diffusion coefficient in interphase boundary:

$$D_i = \frac{3D_{\text{eff}}}{2s g_i} \sim 1.5 \times 10^4 D_{\text{eff}}. \quad (6)$$

In Eq. (6),  $g_i \sim 1.5 \times 10^{-4}$  was estimated with  $\delta \sim 5 \times 10^{-10}$  m [47] and  $s = 1$ . Since it can be expected that both the above conditions, (i) and (ii), are fulfilled, the Eq. (6) can be taken as a useful assessment of  $D_i$ .

## 4. Summary

In the present paper, hydrogen diffusion coefficients in intermetallic compound MgH<sub>2</sub>, and in hydrogen-charged eutectic (Mg + Mg<sub>2</sub>Ni)-H were measured. The hydrogen desorption experiments were done far from the equilibrium, so that the driving force for the hydrides decomposition was high enough and release of hydrogen was controlled by out-diffusion from the hydride phase only. Coefficients of hydrogen diffusion in charged Mg are much lower than values reported in the literature for the hydrogen diffusion in pure Mg. Coefficients of hydrogen diffusion in cast eutectic alloy seem to be effective coefficients characterizing the effective diffusion in a two-phase alloy with high-diffusivity interphase boundaries. Hydrogen diffusion coefficients in interphase boundaries,  $D_i$ , were assessed.

## Acknowledgements

This work was supported by the Czech Science Foundation – contract Nr. 106/07/0010 and by the Czech

Academy of Sciences, project Nr. AV0Z20410507. Authors would like to thank to Mr. B. David, PhD for XRD measurements.

### References

- [1] AVEDESIAN, M. M.—BAKER, H.: Magnesium and Magnesium Alloys. ASM International Materials Park, OH 44073-0002, 1999.
- [2] LUKÁČ, P.—KOCICH, R.—GREGER, M.—PADALKA, O.—SZÁRAZ, Z.: *Kovove Mater.*, **45**, 2007, p. 115.
- [3] DOBROŇ, P.—BOHLEN, J.—CHMELÍK, F.—LUKÁČ, P.—LETZIG, D.—KAINER, K. U.: *Kovove Mater.*, **45**, 2007, p. 129.
- [4] BALÍK, J.—LUKÁČ, P.—BOHLEN, J.—KAINER, K. U.: *Kovove Mater.*, **45**, 2007, p. 135.
- [5] TROJANOVÁ, Z.—MILNERA, M.: *Kovove Mater.*, **44**, 2006, p. 75.
- [6] TROJANOVÁ, Z.—LUKÁČ, P.: *Kovove Mater.*, **43**, 2005, p. 73.
- [7] JANEČEK, M.—ŠUPÍK, V.—HOLLÄNDER, F.—WENDT, J.: *Kovove Mater.*, **43**, 2005, p. 218.
- [8] MATHIS, K.—TROJANOVÁ, Z.: *Kovove Mater.*, **43**, 2005, p. 238.
- [9] HNILICA, F.—OČENÁŠEK, V.—STULÍKOVÁ, I.—SMOLA, B.: *Kovove Mater.*, **43**, 2005, p. 300.
- [10] JÄGER, A.—LUKÁČ, P.—GÄRTNEROVÁ, V.: *Kovove Mater.*, **42**, 2004, p. 165.
- [11] TRUDEAU, M. L.: *MRS Bull.*, **24**, 1999, p. 23.
- [12] ROSS, D. K.: *Vacuum*, **80**, 2006, p. 1084.
- [13] BÉRUBÉ, V.—RADTKE, G.—DRESSELHAUS, M.—CHEN, G.: *Int. J. Energ. Res.*, **31**, 2007, p. 637.
- [14] BARKHORDARIAN, G.—KLASSEN, T.—BORMAN, R.: *Scripta Mater.*, **49**, 2003, p. 213.
- [15] BLOMQVIST, H.—RÖNNEBRO, E.—NORÉUS, D.—KUJI T.: *J. Alloy Compd.*, **330**, 2002, p. 268.
- [16] KOJIMA, Y.—KAWAI, Y.—HAGA, T.: *J. Alloy Compd.*, **424**, 2006, p. 294.
- [17] MONTONE, A.—ANTISARI, M. V.—ABAZOVIĆ, N.—NOVAKOVIĆ, J. G.—PASQUINI, L.—BONETTI, E.—FIORINI, A. L.: *Mat. Sci. For.*, **555**, 2007, p. 335.
- [18] SCHWARTZ, R. B.: *MRS Bull.*, **24**, 1999, p. 40.
- [19] GAO, R. G.—TU, J. P.—WANG, X. L.—ZHANG, X. B.—CHEN, C. P.: *J. Alloy Compd.*, **356**, 2003, p. 649.
- [20] MARTIN, M.—GOMEL, C.—BORKHART, C.—FROMM, E.: *J. Alloy Compd.*, **238**, 1996, p. 193.
- [21] FERNÁNDEZ, G. E.—RODRÍGUEZ, D.—MAYER, G.: *Int. J. Hydrogen Energ.*, **293**, 1998, p. 1193.
- [22] FANG, S.—ZHOU, Z.—ZHANG, J.—YAO, M.—FENG, F.—NORTHWOOD, D. O.: *J. Alloy Compd.*, **293**, 1999, p. 10.
- [23] LIANG, G.—HUOT, J.—BOILY, S.—SCHULZ, R. J.: *Alloy Comp.*, **305**, 2000, p. 239.
- [24] FERNÁNDEZ, J. F.—SANCHEZ, C. R.: *J. Alloy Compd.*, **340**, 2002, p. 189.
- [25] GABIS, I. E.—VOIT, A. P.—EVARD, E. A.—ZAIKA, Y. U. V.—CHERNOV, I. A.—YARTIS, V. A.: *J. Alloy Compd.*, **404**, 2005, p. 312.
- [26] LI, Q.—LIN, Q.—CHOU, K. C. H.—JIANG, L.: *J. Mater. Sci.*, **39**, 2004, p. 61.
- [27] CHOU, K.-C.—XU, K.: *Intermetallics*, **15**, 2007, p. 767.
- [28] CHOU, K.-C.—LI, Q.—LIN, Q.—JIANG, L.-J.—XU, K.-D.: *Int. J. Hydrogen Energ.*, **30**, 2005, p. 301.
- [29] RUDMAN, P. S.: *J. Appl. Phys.*, **50**, 1979, p. 7195.
- [30] GAVRA, Z.—MINTZ, M. H.: *Inorg. Chem.*, **18**, 1979, p. 3595.
- [31] HAYAKAWA, H.—ISHIDO, Y.—NOMURA, K.—URUNO, H.—ONO, S.: *J. Less-Common Met.*, **103**, 1984, p. 277.
- [32] NORÉUS, D.—KIHLBORG, L.: *J. Less-Common Met.*, **123**, 1986, p. 233.
- [33] ZOLLIKER, P.—YVON, K.—BEARLOCHER, CH.: *J. Less-Common Met.*, **115**, 1986, p. 65.
- [34] POST, L. M.—MURRAY, J. J.: *J. Less-Common Met.*, **134**, 1987, p. 15.
- [35] SELVAM, P.—VISWANATHAN, B.—SWAMY, C. S.—SRINIVASAN, V.: *Int. J. Hydrogen Energ.*, **13**, 1988, p. 749.
- [36] HAYASHI, S.—HAYAMIZU, K.: *J. Less-Common Met.*, **155**, 1989, p. 31.
- [37] DARNAUDERY, J. P.—PEZAT, M.—DARRIET, B.—HAGENMULLER, P.: *Mater. Res. Bull.*, **16**, 1981, p. 1237.
- [38] BLOMQVIST, H.—NORÉUS, D.: *J. Appl. Phys.*, **91**, 2002, p. 5141.
- [39] BLOMQVIST, H.—NORÉUS, D.—BABUSHKIN, O.—NION, F.—VOURIEN, E.: *J. Mater. Sci. Lett.*, **22**, 2003, p. 1487.
- [40] KIM, W. G.—UR, S. C.—LEE, Y. G.—KIM, Y. J.—HONG, T. W.: *Mat. Sci. For.*, **544**, 2007, p. 311.
- [41] ICSD Database release 2007/1, FIZ Karlsruhe, Germany.
- [42] JCPDS PDF-4 Full File 2004 Database, ICDD, Newton Square, Pennsylvania, U.S.A.
- [43] X'Pert HighScore Plus 2.0a, PANanalytical B. V., Almelo, the Netherlands.
- [44] SANDROCK, G. D.—SUDA, S.—SCHLAPBACH, L.: In: *Hydrogen in Intermetallic Compounds*. Vol. II. Chapter 5. Ed.: Schlapbach, L. Berlin, Springer 1992.
- [45] CARSLAW, H. S.—JAEGER, J. C.: *Conduction of Heat in Solids*. Oxford, Clarendon Press 1959.
- [46] CRANK, J.: *Mathematics of Diffusion*. Oxford, Clarendon Press 1957.
- [47] KAUR, I.—MISHIN, Y.—GUST, W.: *Fundamentals of Grain and Interphase Boundary Diffusion*. Chichester, New York, Brisbane, Toronto, Singapore, John Wiley & Sons Ltd. 1995.
- [48] RENNER, J.—GRABKE, H. J.: *Z. Metallkd.*, **69**, 1978, p. 639.
- [49] SCHIMMEL, H. G.—KEARLEY, G. J.—HUOT, J.—MULDER, F. M.: *J. Alloy Compd.*, **404**, 2005, p. 235.
- [50] NISHIMURA, C.—KOMAKI, M.—AMANO, M.: *J. Alloy Compd.*, **293**, 1999, p. 329.
- [51] SENEGAS, J.—MIKOU, A.—PEZAT, M.—DARIET, B.: *J. Solid State Chem.*, **52**, 1984, p. 1.
- [52] TOEPLER, H.—BUCHNER, H.—SAEUFFERER, K.—KNORR, K.—PRANDL, W.: *J. Less-Common Met.*, **88**, 1982, p. 397.
- [53] HAYASHI, S.—HAYAMIZU, K.—YAMAMOTO, O.: *J. Phys. Chem. Solids*, **45**, 1984, p. 555.
- [54] BELOVA, I. V.—MURCH, G. E.: *Phil. Mag.*, **84**, 2004, p. 17.